Supplemental Material: Electronic character of charge order in square planar low valence nickelates

Y. Shen,* J. Sears, G. Fabbris, J. Li, J. Pelliciari, M. Mitrano, W. He, Junjie Zhang, J. F. Mitchell, V. Bisogni, M. R. Norman, S. Johnston, and M. P. M. Dean†

(Dated: January 29, 2023)

I. ABSENCE OF DIAGONAL CHARGE ORDER IN $Pr_4Ni_3O_8$

To confirm the absence of diagonal charge order in metallic $Pr_4Ni_3O_8$ [1], we performed resonant inelastic x-ray scattering (RIXS) measurements near $\mathbf{Q}_\parallel = (1/3, 1/3)$ in $Pr_4Ni_3O_8$. Figure S1 shows the RIXS spectra in the quasi-elastic regime with σ polarized incident photons. No superlattice peaks are found but only background evolving smoothly with the in-plane sample angle θ, which is primarily caused by the self-absorption effect. Note that despite the absence of long-range or short-range stripe order indicated here, stripe related spin fluctuations are distinguished in the inelastic regime [2].

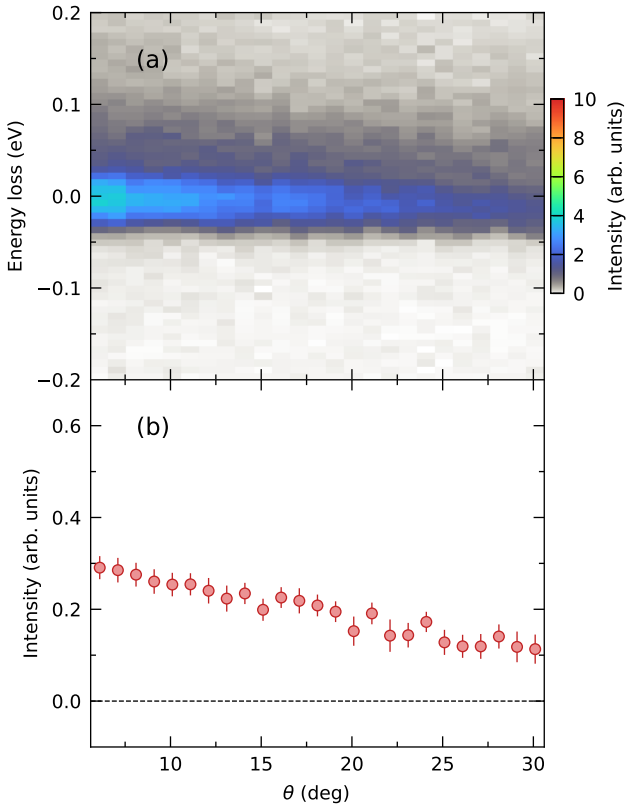

FIG. S1. Absence of charge order in $Pr_4Ni_3O_8$ at 40 K. (a) RIXS intensity map around $\mathbf{Q}_\parallel = (1/3, 1/3)$ in the quasi-elastic regime at the Ni L_3-edge. The experimental configuration is the same as that for $La_4Ni_3O_8$. (b) Quasi-elastic amplitudes extracted from (a).

* yshen@bnl.gov
† mdean@bnl.gov

II. RIXS PROCESS FOR DIFFERENT EXCITATIONS

Here we discuss the RIXS process for different excitations. Due to the presence of the strong core-hole potential in the RIXS intermediate states, the electron that is excited from the core level is constrained to a few unit cells near the Ni site where the x-ray absorption takes place. This effect competes with the kinetic energy of the electron and leads to intertwined excitations in the RIXS spectra. In a simplified picture, the orbital states during the RIXS process can be divided into three categories based on how they are affected by the core-hole potential [see Fig. S2(a)]. The first one involves the Ni $3d$ orbitals that are strongly localized at the core-hole site. The second one involves the ligand orbitals that surround the Ni site and strongly hybridize with the Ni $3d$ orbitals. They are largely localized but could show a finite bandwidth. The third one involves continuous electronic bands that are mostly unperturbed by the core-hole potential and behave itinerantly with an appreciable bandwidth. The localized Ni $3d$ orbitals can hybridize with the continuous bands in an orbital dependent fashion. At the Ni L-edge, the core electron is predominantly excited to the unoccupied localized Ni $3d$ orbitals [see Fig. S2(b)]. During the photon emission process, either an electron from another $3d$ orbital deexcites to fill the core hole, leading to dd multiplet excitations [see Fig. S2(d)], or an electron from the ligand orbitals hops to the Ni site, resulting in charge-transfer excitations [Fig. S2(e)]. Since the ligand orbitals normally lie at a lower energy, the charge-transfer excitations usually occur with a larger energy loss than the dd excitations and are much weaker at the Ni L-edge as they are made possible through hybridization. In the post-edge regime, the core electron is excited to the unoccupied states in the continuous bands through hybridization in the intermediate state [see Fig. S2(c)], and during the photon emission an electron below the Fermi level deexcites to fill the core hole, leading to the fluorescence [see Fig. S2(f)]. As the deexciting process is dominated by electrons near the Fermi energy, fluorescence tends to present a constant emission photon energy. Note that at the Ni L-edge RIXS process, contributions from rare earth and oxygen states are seen via their hybridization with atomic Ni $3d$ orbitals. In real materials, there are no clear boundaries between the localized orbitals and continuous bands. Thus, different excitations are also intertwined but the weights are quite different, which helps us distinguish them in the RIXS spectra.

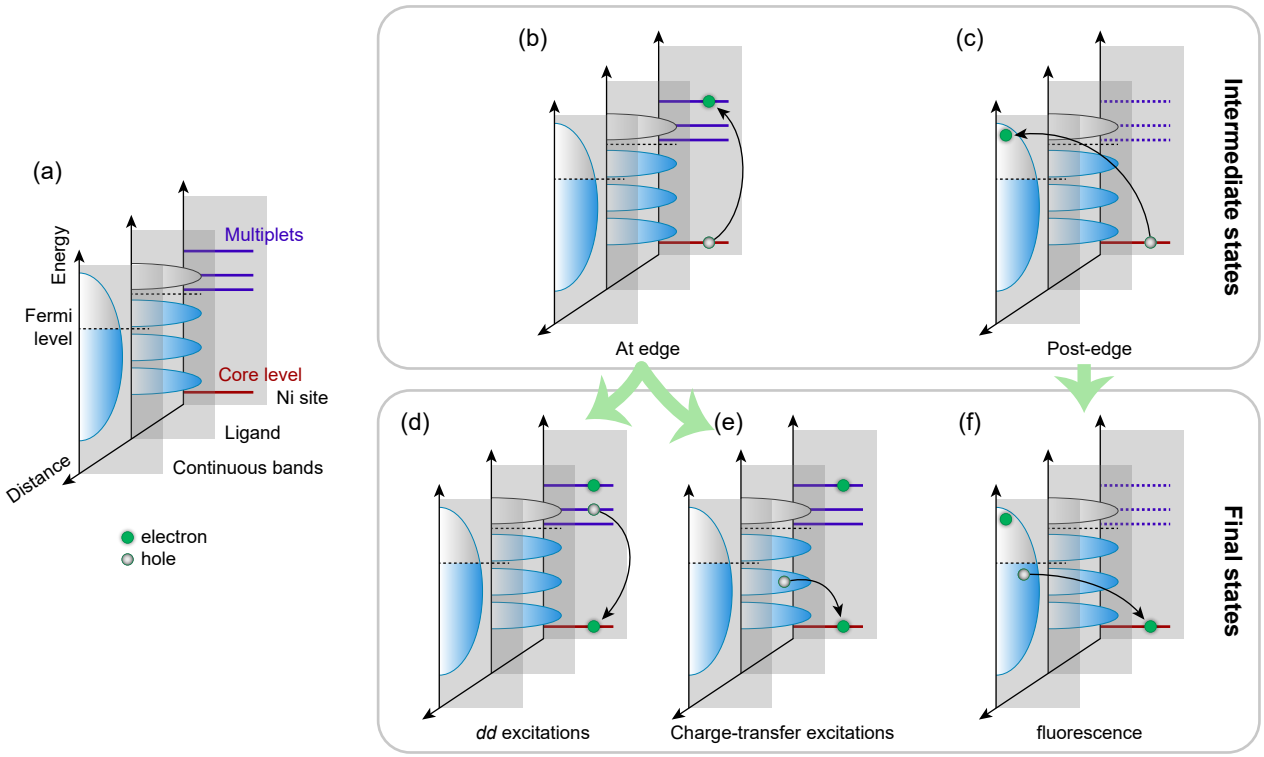

FIG. S2. RIXS process for different excitations. (a) Legend for each symbol. (b, c) Photon absorption process and corresponding intermediate states. (d)–(f) Photon emission process and corresponding final states. For the fluorescence excitation scenario, the multiplets are not well defined so they are replaced by dashed lines.

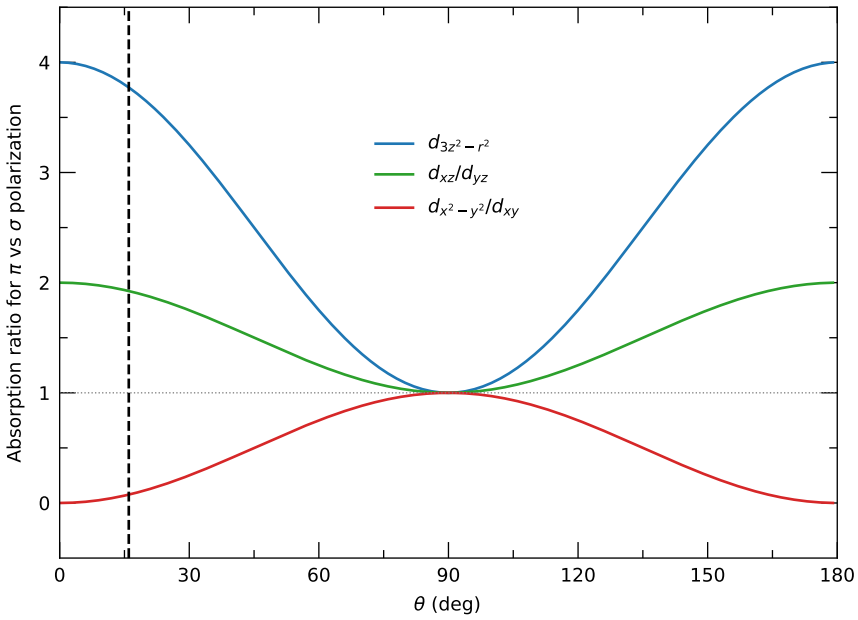

FIG. S3. Intensity ratio for dipole absorption between π and σ polarization channels as a function of sample angle θ. The vertical dashed line indicates the experimental configuration we used for charge order measurements while the horizontal dotted line denotes a unit ratio.

III. POLARIZATION DEPENDENCE OF FLUORESCENCE

The polarization dependence of *dd* excitations in cuprates and nickelates has been widely discussed [3, 4]. Here, we focus on fluorescence to show how the orbital information can be extracted by comparing the RIXS intensity in different polarization channels. Since we are measuring at the Ni L edge, the RIXS signal can only arise from either Ni orbitals or Ni states hybridized with other orbitals. For the fluorescence features, the photon emission process is quite similar, with electrons from the crystalline environment surrounding the Ni site deexciting to fill the core hole. Hence, the main intensity difference between these two polarization channels comes from the photon absorption process, the cross-section of which can be simulated in the dipole approximation. Fig. S3 presents the x-ray dipole absorption intensity ratio between π and σ polarization channels as a function of sample angle θ. For the experimental configuration we used (vertical dashed line), the biggest contribution to the π over σ polarization intensity ratio is the Ni $3d_{3z^2-r^2}$ orbitals while $3d_{x^2-y^2}$ and $3d_{xy}$ contribute equally to the σ over π polarization intensity ratio. Since the $3d_{x^2-y^2}$ orbitals dominate near the Fermi level and are expected to show stronger hybridization with oxygen orbitals [5], $3d_{xy}$ orbitals are expected to play a less important role. Moreover, the t_{2g} states do not make any significant contribution to the unoccupied states. Thus, we focus on Ni e_g orbitals during the discussion in the main text, which are the subject of most of the debates over the appropriate theoretical models.

IV. MINIMAL CONTRIBUTION OF SPIN ORDER TO THE REXS SIGNAL

In $La_4Ni_3O_8$, spin order takes place concomitantly with the charge order and shares the same $\mathbf{Q}_\parallel$. Hence we need to invoke cross-section considerations to separate the possible contribution of charge and spin order [6].

With π incident x-ray polarization, charge order contributes to the measured signal in the π-π' scattering channel while the spin order is responsible for the π-σ' channel. The resonant elastic x-ray scattering (REXS) intensity ratio between these channels can be estimated by $(\boldsymbol{k}_i \cdot \boldsymbol{k}_f)^2/(\boldsymbol{\epsilon}_i \times \boldsymbol{\epsilon}'_f \cdot \boldsymbol{M})^2 = \cos^2 2\Theta/\sin^2\theta \approx 11.8$, where $\boldsymbol{k}_i$ ($\boldsymbol{k}_f$) is the initial (final) x-ray wavevector, $\boldsymbol{\epsilon}_i$ ($\boldsymbol{\epsilon}'_f$) is the initial (final) x-ray polarization, and $\boldsymbol{M}$ is the spin direction, which is parallel to the c-axis in this case. Based on this formula we can see that the REXS signal with π incident polarization is dominantly of charge order origin.

Regarding the spin order contribution with σ incident x-ray polarization, we can compare the peak intensity with grazing-in and grazing-out conditions. Since the charge order composes the σ-σ' channel, its intensity is expected to be the same in these two geometries. For spin order signal that is only observable in the σ-π' channel, the intensity

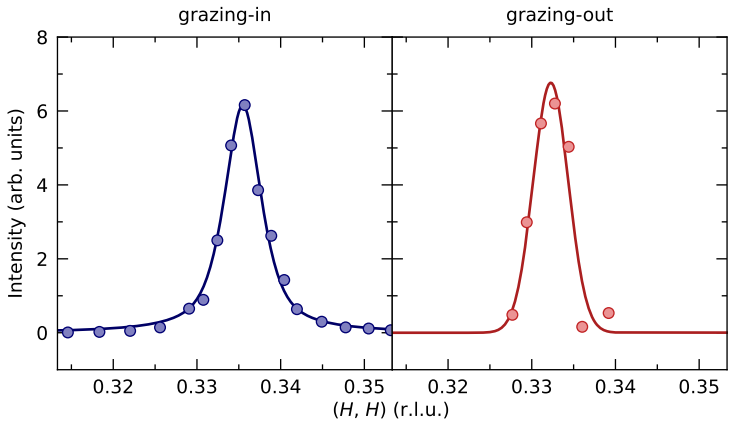

FIG. S4. Comparison of the superlattice peak intensity with grazing-in and grazing-out conditions. The scattering angle 2Θ was fixed to 153° and the data were collected in σ polarization channel at 40 K. The solid lines are guides to the eye. Both peaks are found to have essentially the same intensity, which confirms that the peak arises from charge, rather than spin, order.

TABLE S1. Full list of parameters used for the ED calculations. The on-site orbital energies, hopping integrals and Coulomb interactions are kept the same as those used in the O K-edge calculations [7], and $V_{pd\pi} = -V_{pd\sigma}/2$, $V_{pp\pi} = -V_{pp\sigma}/4$. The potential difference, $\Delta\epsilon_d$, only applies to the Ni $3d$ orbitals. Note that the crystal field splitting that is instead used in a Ni atomic model is a combination of point charge potential and orbital hybridization, which can be estimated through ligand field theory [5]. The resulting effective crystal field splitting gives $10D_q = 0.971$, $\Delta e_g = 1.041$, $\Delta t_{2g} = 0.342$ eV, which are of a similar energy scale as the dd excitations observed in the RIXS measurements. $\zeta_{\rm i}$ and $\zeta_{\rm n}$ are spin-orbit coupling parameters of the Ni $3d$ electrons for the initial and intermediate states, respectively, and $\zeta_{\rm c}$ is the spin-orbit coupling strength for the Ni $2p$ core electrons. The core-hole lifetime is set to be 0.6 eV. All parameters are in units of eV.

On-site orbital energies							Hopping integrals	
$\epsilon_{d_{x^2-y^2}}$	$\epsilon_{d_{3z^2-r^2}}$	$\epsilon_{d_{xy}}$	$\epsilon_{d_{xz/yz}}$	ϵ_{p_σ}	ϵ_{p_π/p_z}		$V_{pd\sigma}$	$V_{pp\sigma}$
0	0.2	0.1	0.3	5.6	6.1		1.57	0.6
Spin-orbit coupling				On-site Coulomb interactions				
$\zeta_{\rm i}$	$\zeta_{\rm n}$	$\zeta_{\rm c}$		F^0_{dd}	F^2_{dd}	F^4_{dd}	F^0_{pp}	F^2_{pp}
0.083	0.102	11.507		5.58	6.89	4.31	3.3	5
Inter-site Coulomb interactions				Core-hole potential				
F^0_{dp}	F^2_{dp}	G^1_{dp}	G^3_{dp}	F^0_{dp}	F^2_{dp}	G^1_{dp}	G^3_{dp}	
1	0	0	0	7.869	5.405	4.051	2.304	

ratio between grazing-in and grazing-out conditions is $(\boldsymbol{k}_{f,\ \text{grazing}-\text{in}} \cdot \boldsymbol{M})^2/(\boldsymbol{k}_{f,\ \text{grazing}-\text{out}} \cdot \boldsymbol{M})^2 \approx 5.6$, indicating that the spin order signal should be strongly suppressed with grazing-out condition. Figure S4 shows the $\mathbf{Q}$ dependence of the superlattice peak with both conditions, which are comparable with each other, proving that the superlattice peak observed with σ incident x-ray polarization is also dominantly of charge order origin.

V. CHARGE ORDER IN ED CALCULATIONS.

We use cluster ED to study the charge order in the low-valence nickelate $La_4Ni_3O_8$. The full list of the parameters used is presented in Table S1. The validity of our cluster model and parameters has been verified by calculating the RIXS energy maps and confirming that they capture the main features of the measurements as shown in the main text. In the calculations, we include all the Ni $3d$ and O $2p$ orbitals, which leads to a large Hilbert space and correspondingly only a limited number of states can be solved for. Fortunately, the accessible energy range covers the dd excitations so that we can make a direct comparison with the experimental data. The calculated results are broadened using a Gaussian profile with a full width at half maximum of 0.3 eV and are shown in Fig. 3 of the main text.

To fully explore the charge order character in the ED calculations, we need to cover a large incident energy range but only the ground state is needed to calculate the REXS signals. Thus, we only include the Ni $3d_{x^2-y^2}$ and O $2p_\sigma$

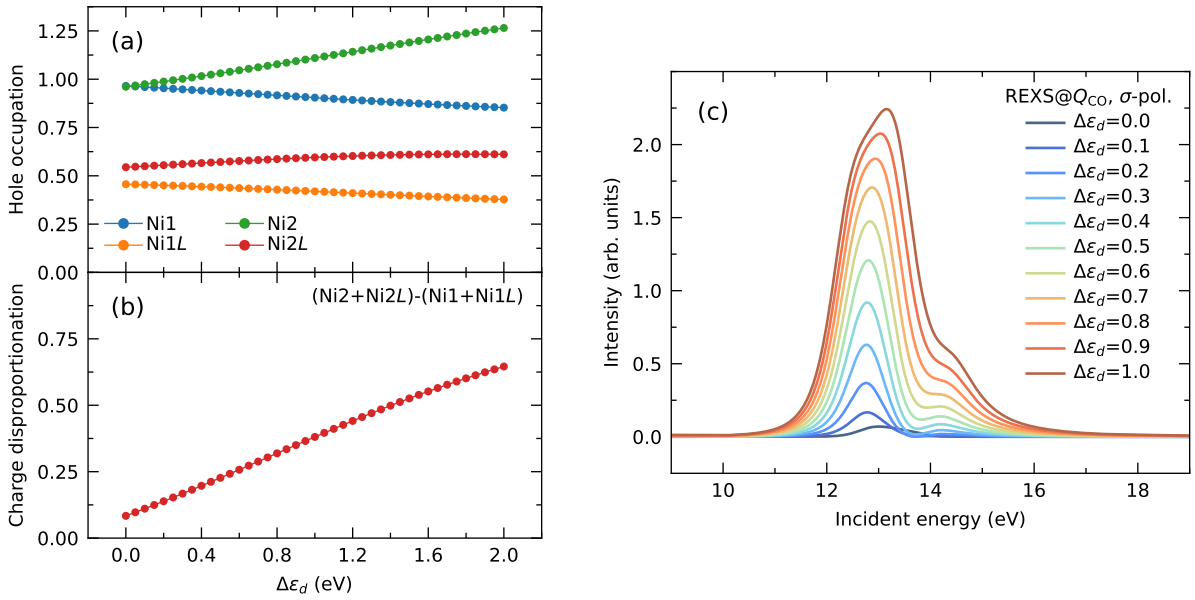

FIG. S5. The emergence of charge order by introducing the potential difference term $\Delta\epsilon_d$. (a) Hole occupations of different sites as a function of $\Delta\epsilon_d$. Ni1L stands for the ligand orbitals for Ni1 (the surrounding four oxygens). Correspondingly, one oxygen is shared by Ni1L and Ni2L. (b) Charge disproportionation defined as the hole occupation difference of Ni1+Ni1L and Ni2+Ni2L. (c) Calculated REXS signals at $\mathbf{Q}_{\mathrm{CO}}$ with different $\Delta\epsilon_d$. All the calculations are performed with $\Delta = 5.6$ eV.

orbitals during the calculations of the charge order, which dominate the ground state, so that a tractable basis size is realized. To trigger charge order in the Ni_3O_{10} cluster, we introduce a potential difference $\Delta\epsilon_d$ as described in the main text. In a microscopic model like we use here, the onsite energy shift and charge occupation are intrinsically coupled, which is different from a phenomenological model where these two factors can be tuned independently [8, 9]. As shown in Fig. S5, when $\Delta\epsilon_d$ is zero, the hole occupations on different Ni sites are almost the same while the hole occupations of ligand orbitals are slightly imbalanced since Ni2 shares oxygens with both Ni1 and Ni3, leading to a small charge disproportionation. With increasing $\Delta\epsilon_d$, the charge imbalances on both the Ni and ligand orbitals are enhanced with the former much more prominent, indicating that most of the spatial charge modulation resides on the Ni sites, leading to a Ni site-centered charge order. Correspondingly, a charge-order peak emerge in the REXS calculations, the intensity of which increases with increasing charge disproportionation while the lineshape only evolves by a little.

After testing the effect of $\Delta\epsilon_d$, here we compare results with different charge-transfer energy Δ in addition to the calculated results presented in the main text. As shown in Fig. S6, in the charge-transfer regime ($\Delta \ll U_{dd}$), a sharp resonant peak is obtained, resembling the experimental observations in cuprates. With increasing Δ, the REXS lineshape evolves correspondingly. In the Mott-Hubbard limit ($\Delta \gg U_{dd}$), the charge order peak becomes broader and shows multiple peak features. Compared with the data presented in the main text, we conclude that a charge-transfer energy with an intermediate strength ($\Delta \approx U_{dd}$) matches the experimental results the best.

[1] Junjie Zhang, A.S. Botana, J.W. Freeland, D. Phelan, Hong Zheng, V. Pardo, M.R. Norman, and J.F. Mitchell, "Large orbital polarization in a metallic square-planar nickelate," Nature Physics **13**, 864–869 (2017).
[2] J. Q. Lin, P. Villar Arribi, G. Fabbris, A. S. Botana, D. Meyers, H. Miao, Y. Shen, D. G. Mazzone, J. Feng, S. G. Chiuzbăian, A. Nag, A. C. Walters, M. García-Fernández, Ke-Jin Zhou, J. Pelliciari, I. Jarrige, J. W. Freeland, Junjie Zhang, J. F. Mitchell, V. Bisogni, X. Liu, M. R. Norman, and M. P. M. Dean, "Strong superexchange in a $d^{9-\delta}$ nickelate revealed by resonant inelastic x-ray scattering," Physical Review Letters **126**, 087001 (2021).
[3] M. Rossi, H. Lu, A. Nag, D. Li, M. Osada, K. Lee, B. Y. Wang, S. Agrestini, M. Garcia-Fernandez, J. J. Kas, Y.-D. Chuang, Z. X. Shen, H. Y. Hwang, B. Moritz, Ke-Jin Zhou, T. P. Devereaux, and W. S. Lee, "Orbital and spin character of doped carriers in infinite-layer nickelates," Physical Review B **104**, L220505 (2021).
[4] M. Moretti Sala, V. Bisogni, C. Aruta, G. Balestrino, H. Berger, N. B. Brookes, G. M. de Luca, D. Di Castro, M. Grioni,

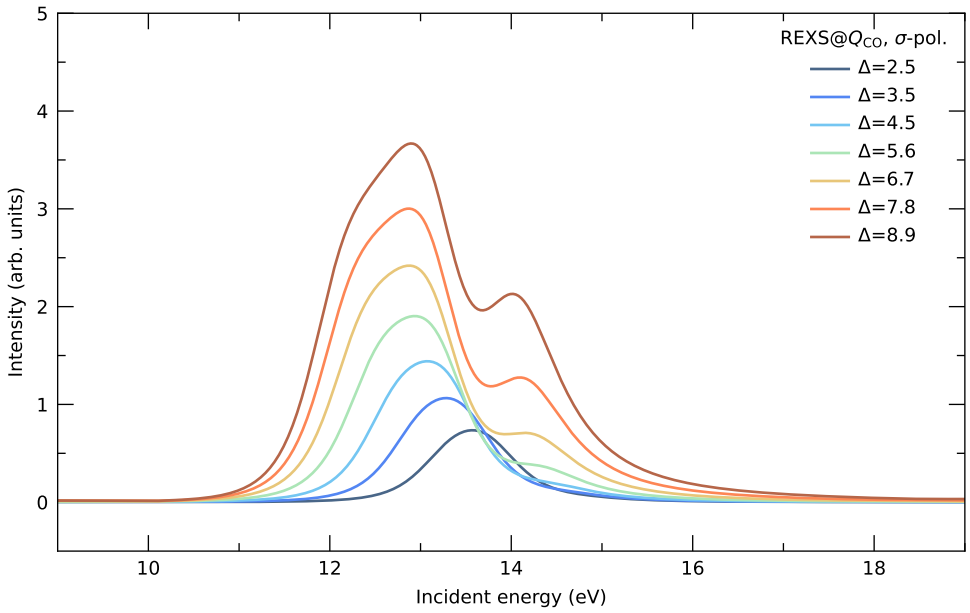

FIG. S6. Calculated REXS signals at the charge order wavevector $\mathbf{Q}_{\mathrm{CO}}$ with different charge-transfer energy Δ. All the calculations are performed with $\Delta\epsilon_d = 0.8$ eV and $U = 6.5$ eV.

M. Guarise, P. G. Medaglia, F. Miletto Granozio, M. Minola, P. Perna, M. Radovic, M. Salluzzo, T. Schmitt, K. J. Zhou, L. Braicovich, and G. Ghiringhelli, "Energy and symmetry of *dd* excitations in undoped layered cuprates measured by Cu L_3 resonant inelastic x-ray scattering," New Journal of Physics **13**, 043026 (2011).

[5] M. W. Haverkort, M. Zwierzycki, and O. K. Andersen, "Multiplet ligand-field theory using wannier orbitals," Physical Review B **85**, 165113 (2012).

[6] M. W. Haverkort, "Theory of resonant inelastic x-ray scattering by collective magnetic excitations," Physical Review Letters **105**, 167404 (2010).

[7] Y. Shen, J. Sears, G. Fabbris, J. Li, J. Pelliciari, I. Jarrige, Xi He, I. Božović, M. Mitrano, Junjie Zhang, J. F. Mitchell, A. S. Botana, V. Bisogni, M. R. Norman, S. Johnston, and M. P. M. Dean, "Role of oxygen states in the low valence nickelate $La_4Ni_3O_8$," Physical Review X **12**, 011055 (2022).

[8] A. J. Achkar, R. Sutarto, X. Mao, F. He, A. Frano, S. Blanco-Canosa, M. Le Tacon, G. Ghiringhelli, L. Braicovich, M. Minola, M. Moretti Sala, C. Mazzoli, Ruixing Liang, D. A. Bonn, W. N. Hardy, B. Keimer, G. A. Sawatzky, and D. G. Hawthorn, "Distinct charge orders in the planes and chains of ortho-III-ordered $YBa_2Cu_3O_{6+\delta}$ superconductors identified by resonant elastic x-ray scattering," Physical Review Letters **109**, 167001 (2012).

[9] A. J. Achkar, F. He, R. Sutarto, J. Geck, H. Zhang, Y.-J. Kim, and D. G. Hawthorn, "Resonant x-ray scattering measurements of a spatial modulation of the Cu 3*d* and O 2*p* energies in stripe-ordered cuprate superconductors," Physical Review Letters **110**, 017001 (2013).